ELSEVIER

Nuclear Engineering and Design 204 (2001) 321–336

Nuclear Engineering and Design

www.elsevier.com/locate/nucengdes

Pressure suppression pool mixing in passive advanced BWR plants

Robert E. Gamble [a,*], Thuy T. Nguyen [a], Bharat S. Shiralkar [a], Per F. Peterson [b], Ralph Greif [c], H. Tabata [d]

[a] *GE Nuclear Energy, 175 Curtner Avenue M/C 365, San Jose, CA 95125, USA*
[b] *Department of Nuclear Engineering, University of California, Berkeley, CA 94720-1730, USA*
[c] *Department of Mechanical Engineering, University of California, Berkeley, CA 94720-1730, USA*
[d] *Japan Atomic Power Company, 1-6-1 Otemachi, Chiyoda-ku, Tokyo 100-0004, Japan*

Received 5 July 2000; accepted 5 July 2000

Abstract

In the SBWR passive boiling water reactor, the long-term post-accident containment pressure is determined by the combination of noncondensible gas pressure and steam pressure in the wetwell gas space. The suppression pool (SP) surface temperature, which determines the vapor partial pressure, is very important to overall containment performance. Therefore, the thermal stratification of the SP due to blowdown is of primary importance. This work looks at the various phases and phenomena present during the blowdown event and identifies those that are important to thermal stratification, and the scaling necessary to model them in reduced size tests. This is important in determining which of the large body of blowdown to SP data is adequate for application to the stratification problem. The mixing by jets from the main vents is identified as the key phenomena influencing the thermal response of the suppression pool and analytical models are developed to predict the jet influence on thermal stratification. The analytical models are implemented into a system simulation code, TRACG, and used to model thermal stratification behavior in a scaled test facility. The results show good general agreement with the test data.

1. Introduction

The new class of advanced reactors relies on passive safety grade containment systems rather than active ones to reduce cost and improve maintainability and reliability. As a result, phenomena that were previously of little or no importance have become important and some systems have received renewed attention, one being the suppression pool (SP) of passive boiling water reactors where pool surface temperature plays an important part in determining the overall long-term containment pressure.

* Corresponding author. Tel.: +1-408-9253352; fax: +1-408-9253991.

E-mail addresses: robert.gamble@gene.ge.com (R.E. Gamble), peterson@nuc.berkeley.edu (P.F. Peterson), hiroaki-tabata@japc.co.jp (H. Tabata).

0029-5493/01/$ - see front matter
PII: S0029-5493(00)00363-0

In the SBWR passive boiling water reactor (Upton et al., 1996), the long-term containment pressure is determined by the combination of non-condensable gas pressure and steam pressure in the wetwell (WW) gas space, the latter governed by the suppression pool surface temperature. While the SBWR does have active safety systems, the safety grade systems are all passive and do not provide active pool mixing. Therefore, the thermal stratification of the SP due to blowdown through the main vents and safety relief valves (SRVs) as well as venting through the PCC vent are of primary importance for licensing calculations. The clearing and subsequent venting of noncondensible gases and steam over a wide range of fluxes and at a variety of submergence depths result in a wide variety of phenomena that can impact the thermal stratification in the suppression pool.

Much work has been done in the past on various aspects of the SP behavior. General Electric (GE) conducted a series of tests that examined the SP behavior during the blowdown period of a loss-of-coolant accident (LOCA). The tests were performed at the pressure suppression test facility (PSTF). These tests provided data on SP behavior at a variety of scales — full scale (Varzaly et al., 1978), one-third area scale (Varzaly et al., 1977) and one-ninth area scale (Varzaly et al., 1980). These tests are collectively referred to as the PSTF tests. The primary emphasis of these tests was on SP mechanical loading, although some data on thermal behavior was also reported. Although blowdown is a violent high-energy period tests have shown that a significant amount of stratification can exist at its conclusion.

Later work looked at the effects of the venting of steam and noncondensibles from the passive containment cooling (PCC) condenser used in the decay heat period by the SBWR and ESBWR (Coddington and Andreani, 1995).

This work studies the various phases and phenomena of the blowdown period of a LOCA and identifies those that are important to thermal stratification of the SP. This is a significant departure from much past work since the phenomena important to thermal stratification are different than those important to structural loading, which has been studied exhaustively in the past. The paper identifies the important phenomena and the scaling necessary to model them in reduced size tests. This is important in determining which of the large body of structural loading tests are adequate for application to the stratification problem. Analytical models are developed for the buoyant jet structures that provide the dominant mechanism for pool mixing and stratification. Analytical models for the SP response must be based on our understanding of free jets, however, the actual situation has closely spaced jets and 3-D effects which are important. Therefore, analytical models provide only qualitative understanding, detailed 3-D modeling is needed for quantitative assessment.

In an effort to evaluate the effectiveness of our analytical models a simplified treatment capturing the main characteristics of the SP behavior is implemented into the TRACG system code and used to predict the behavior of one of the PSTF tests. A simplified set of models is appropriate for application in large control volume system codes like TRAC and RELAP.

2. Suppression pool transient phases and analysis

This section reviews the possible causes of stratification in the suppression pool, identifies which ones are important and describes analytical models developed to capture the primary characteristics of the SP thermal behavior.

Fig. 1 shows the containment and main vent system for the SBWR. Fig. 2 shows the behavior of key main vent parameters throughout the phases of the blowdown portion of a LOCA. When a LOCA occurs, steam or high-energy liquid is injected into the drywell (DW) resulting in rapid pressurization of the DW, which in turn causes a rapid clearing of the main vent system. Initially there is a water level in the vertical portion of the vent as shown in Fig. 1 During the initial blowdown, the liquid is forced from the vents sending jets of water into the suppression pool. Vent clearing time is on the order of 2 s. This is followed by an injection of noncondensible gases and steam. The noncondensible concentra-

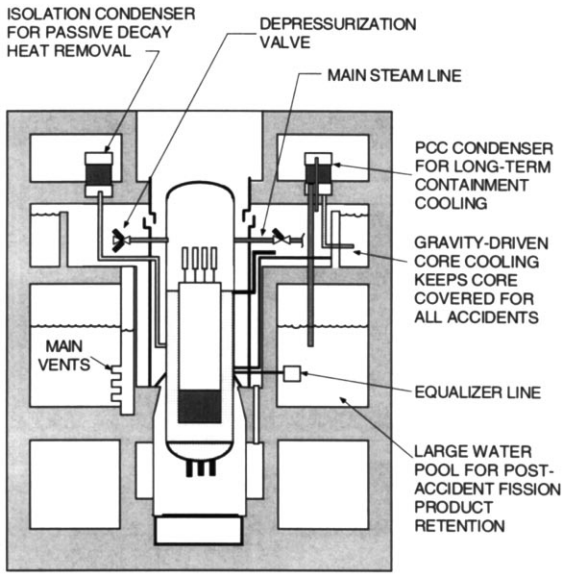

Fig. 1. Containment and main vents.

tion decreases rapidly from 100% to less than 10% in approximately 10 s. Following this, there is a longer period of injection of a mixture rich in steam. The steam injection period can last many minutes. The next subsections provide a review of these phases of a LOCA transient and analytical descriptions of the important phenomena present.

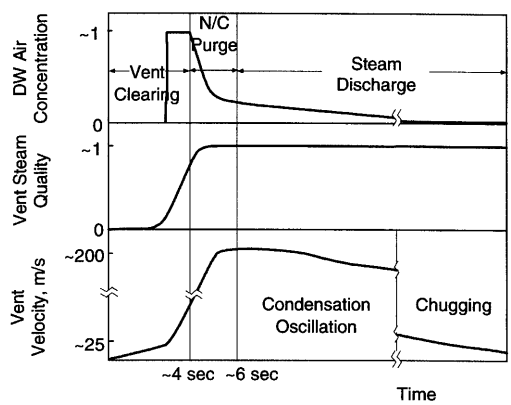

Fig. 2. Characterization of suppression pool and main vent behaviour.

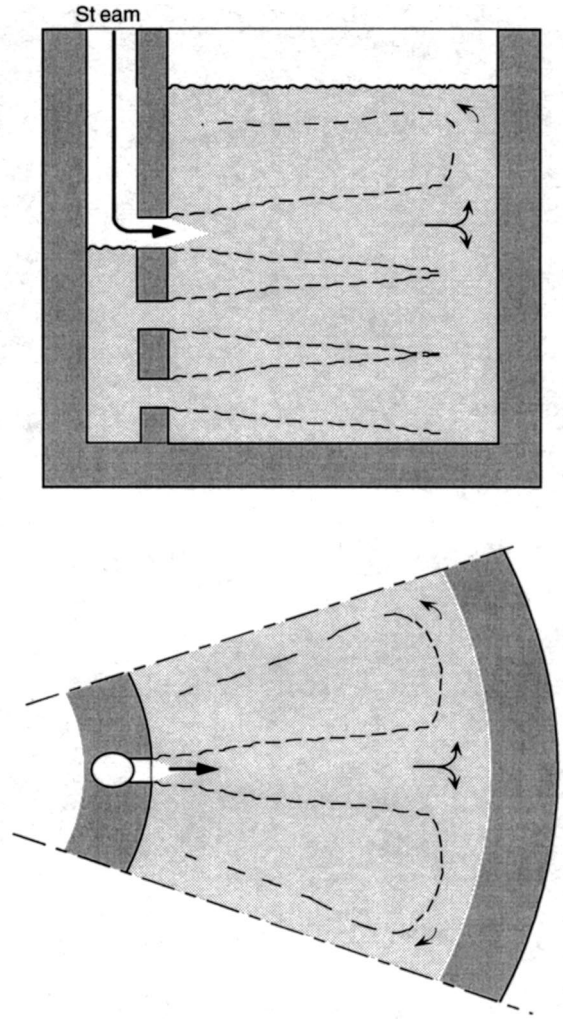

Fig. 3. Jet trajectory in suppression pool.

2.1. Vent clearing

The initial clearing of the water in the vents results in transient jets of liquid that traverse the pool. When each jet reaches the far wall it forms a radial wall jet spreading in all directions (Fig. 3). The behavior is complicated by the fact that the jet is transient (a starting jet) and by the fact that adjacent jets may interact with each other. In the SBWR, there are eight to ten sets of main vents circumferentially spaced 36–45° apart, each containing three vertically-stacked vents. The degree to which the jets overlap when they reach the

far pool wall depends on the width of the pool. Some fraction of the jet will move up along the wall to the surface of the pool and come back across the pool surface.

The behavior of jets has been studied extensively and there are very good integral correlations supported by experimental results for their behavior. Below, correlations are used from the literature to estimate the velocity, width and entrainment rates of forced jets.

2.1.1. Buoyant jet characterization

The jet Reynolds number determines the basic character of the jet

$$Re_{\text{jet}} = \frac{\rho u_{\text{o}} D_{\text{o}}}{\mu} \tag{1}$$

For Reynolds numbers greater than a few thousand, the jet will be turbulent (Rajaratnam, 1976). This is the case for the jets encountered in the SP. As described later, the short period of high noncondensible injection is not considered in detail. For steam injection, condensation occurs over a short distance and the jet is single phase over most of its length. The jet Reynolds number for this case is calculated based on the conditions in the single-phase region just downstream of the condensation section. Table 1 shows Reynolds numbers for the PSTF test and the SBWR.

If the jet is warmer than the pool or contains steam or noncondensible gases, it will be buoyant. The balance between the buoyancy and inertia will determine whether each jet behaves as a forced jet or a plume. The Richardson number characterizes the transition

$$Ri = \frac{Gr}{Re^2} = \left(\frac{\rho_{\text{a}} - \rho_{\text{jet}}}{\rho_{\text{a}}}\right)\frac{gD_{\text{o}}}{u_{\text{o}}^2} \tag{2}$$

where

$$Gr = g\left(\frac{\rho_{\text{a}} - \rho_{\text{jet}}}{\rho_{\text{a}}}\right)\frac{D_{\text{o}}^3}{v^2} \tag{3}$$

is the Grashof number.

As the jet moves across the pool and entrains liquid from the pool, the jet maximum velocity and average temperature decrease. The inertia decreases faster than the buoyancy, however, and at some point, buoyancy becomes important. The jet transitions to buoyant behavior at a distance

$$x_{\text{trans}} = \left(\frac{\pi}{2}\right)^{1/2}\frac{D_{\text{o}}}{Ri^{1/2}} \tag{4}$$

from its discharge point (Gebhart et al., 1988). For the conditions during vent clearing and the majority of the steam discharge phases, the Richardson number is much less than 1 and the resulting transition distance is longer than the pool width so that the jet will behave as a forced jet all the way across the pool with very little upward motion due to buoyancy. Table 1 gives the values for the SBWR and test. The next sections describe the details of the transport process for forced jets.

Table 1
Scaling parameter comparison

Top–down parameters	SBWR	1/3 Scale 5807	Bottom–up Parameters	Vent clearing phase		Steam/noncondensible phase	
				SBWR	1/3 Scale 5807	SBWR	1/3 Scale 5807
$\Delta E_{\text{RPV}}/E_{\text{pool capacity}}$	0.26	0.16	Re_{jet}	5.6E6	3.2E6	3.5E7	4.6E6
$\Delta m_{\text{RPV}}/m_{\text{pool}}$	0.07	0.045	τ_{jet}, s	5.4	1.8	6.9	1.3
$\dot{m}_{\text{RPV}}/m_{\text{pool}}$, s^{-1}	0.0007	0.0016	Ri_{jet}	–[a]	0.005	0.0046	0.0007
$\dot{E}_{\text{RPV}}/E_{\text{pool capacity}}$, s^{-1}	0.0025	0.0014	Ri_{pool}	–[a]	0.15	0.045	0.02
$V_{\text{jet}}/V_{\text{pool}}$	0.059	0.046	Fr_{imp}	1.4	0.85	1.1	1.2
			Fr_{surf}	–[a]	4.6	4.6	6.7

[a] Vent liquid is not expected to be heated above SP temperature in SBWR.

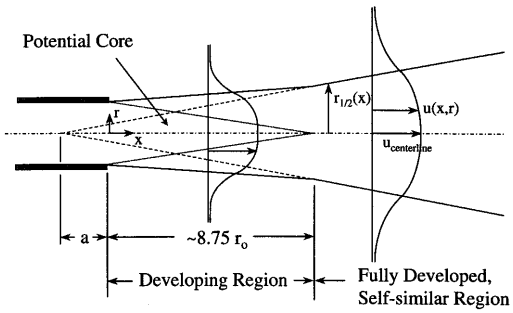

Fig. 4. Developing and fully developed regions of a jet.

2.1.2. Forced turbulent jets

Unbounded, non-buoyant, steady jets are characterized by constant momentum flux along their length. The first portion of a jet is an entry region where the jet velocity and radius vary only slightly. This region extends to approximately four to five jet diameters downstream. Within this region, the shear layer between the fast moving jet and ambient pool fluid is expanding to reach the centerline of the jet (Fig. 4). At a distance of four to five jet diameters the shear layer has reached the centerline and the potential core of the jet has disappeared. In this entrance region the rate of jet expansion is slower than in the fully developed region. The development given by Gauntner et al. (1970) for this region can be linearized to get the following relations for the jet centerline and radius.

$$u_{\text{centerline}} = u_o \quad \text{for } \frac{x}{r_o} \le 8.75 \tag{5}$$

$$\frac{r_{1/2}(x)}{r_o} = \left(1 + 0.013\,\frac{x}{r_o}\right) \tag{6}$$

Here, the end of the entry region has been selected as $x/r_o = 8.75$ which falls within the range of different experimental data. The results are not very sensitive to this selection. The radius, $r_{1/2}$, is based on the point where the velocity is equal to one half the centerline velocity.

Beyond this entry region, an unbounded jet assumes a self-similar profile. Hinze (1959) has shown that the centerline velocity decays hyperbolically with axial distance in this region. Schlichting (1960) suggests that the jet grows linearly with axial distance in this region with a growth rate of $dr/dx = 0.0848$ for the jet half width. Matching this with Eq. (6) at $x/r_o = 8.75$ yields the relation.

$$\frac{r_{1/2}(x)}{r_o} = 0.848\left(4.39 + \frac{x}{r_o}\right) \tag{7}$$

Schlichting also gives the rate of centerline velocity decay as

$$\frac{u_{\text{centerline}}(x)}{u_o} = \frac{13.14}{(a + x/r_o)} \quad \text{for } \frac{x}{r_o} > 8.75 \tag{8}$$

where a is the distance from the virtual origin to the beginning of the jet and is equal to 4.39 from Eq. (7). The axial velocity variation with radial distance has been matched well with several different profiles including the Gaussian error curve and cosine curve. The form recommended by Schlichting is used here,

$$\frac{u(x,r)}{u_{\text{centerline}}} = \left(\frac{1+\eta^2}{4}\right)^{-2} \tag{9}$$

where $\eta = 1.56(r/x)$.

The entrainment by the jet as it moves across the pool is given by (Peterson, 1994)

$$\frac{Q_e}{Q_o} = 2\sqrt{2}\alpha_t\,\frac{x}{r_o} \tag{10}$$

where Q_o is the initial flow rate and α_t is Taylor's entrainment coefficient which has a value of about 0.05. The suppression pool has an x/r_o of about sixteen so the entrainment by the jet as it crosses the pool is about $Q_e/Q_o = 2.3$.

These relations are for individual steady jets traveling in an unconfined space. These assumptions are challenged by the geometry of the suppression pool where interactions with walls and other jets occur. For typical conditions in an SBWR blowdown flow, the superposed velocity profile for three vents is shown in Fig. 5. As indicated, there is an overlap between the jets. The cumulative jet looks more like a rectangular jet. Experiments have shown that in this region for a rectangular jet, there is no growth in the vertical direction and the jet expands in the horizontal direction linearly with distance, similar to a plane jet (Sfier, 1976). This velocity decay is slower than for an axisymmetric jet (proportional

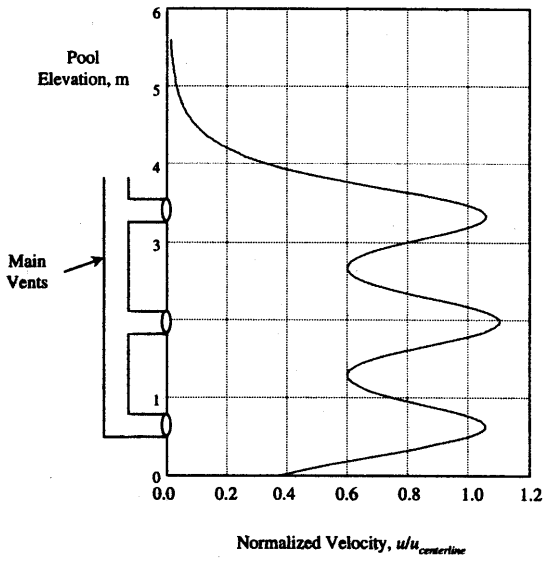

Fig. 5. horizontal velocity profile of vent discharge jets approaching the far wall.

to square root of distance rather than linear with distance). There will be some additional smoothing of the velocity profile to reduce the peaks along the centerlines of the original jets so the centerline velocity can be expected to decay at a rate between an axisymmetric jet and a rectangular one. In the current analysis, the axisymmetric approximations above are used. When a jet hits the far vertical wall, it will expand into a radial jet moving out along the wall in all directions (Poreh et al., 1967, Fig. 6). This motion will also be limited by the expansion of adjacent jets. The maximum velocity in the wall jet from a perpendicularly impinging round jet is given as (Dodge and Ricker, 1978)

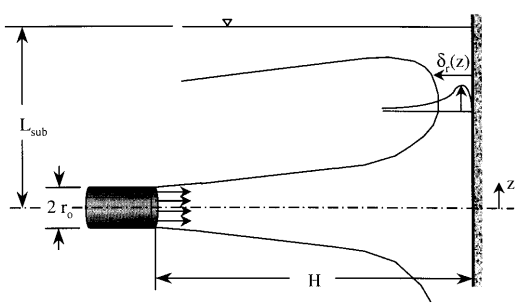

Fig. 6. Impinging jet.

$$\frac{u_r}{u_o} = \frac{3.08}{(z/r_o)^{1.12}} \quad \text{for } z > 0.4H \tag{11}$$

where u_o is the velocity at the original jet source, H the distance from the jet source to the wall (i.e. the pool length) and z is the distance along the wall from the impingement stagnation point. Poreh et al. (1967) gives a similar relation, although theirs has a slight dependence on the height-to-diameter ratio, H/r_o, not seen in Eq. (11). Poreh et al. also give a relation for the jet thickness as

$$\frac{\delta_r}{H} = 0.098\left(\frac{z}{H}\right)^{0.9} \tag{12}$$

Using the results above for the impinging round jet, the jet maximum velocity and thickness of the radial jet when it reached the surface of the pool, if undisturbed by the surface, would be

$$\frac{u_r(L_{sub})}{u_o} = \frac{3.08}{(L_{sub}/r_o)^{1.12}} = 0.2 \tag{13}$$

and

$$\frac{\delta_r}{H} = 0.098\left(\frac{L_{sub}}{H}\right)^{0.9} = 0.1 \tag{14}$$

where L_{sub} is the submergence of the jet when it impinges on the wall.

If the jet is very strong when it hits the surface, it will cause surface waves that will quickly dissipate the jet energy. This interaction is governed by the impingement Froude number (Jirka and Harleman, 1979)

$$Fr_{imp} = \left(\frac{u^2}{g(\delta_r/2)}\right) \tag{15}$$

For small surface Froude numbers there are very little surface interactions and the pool surface acts as a wall. For the purposes of this analysis the, effects of surface waves are neglected and the surface is assumed to act as a solid wall with no friction.

The jet will next spread along the surface of the pool. Jirka and Harleman (1979) show that for forced jets, the non-dimensional surface layer thickness, t/L_{sub}, falls in the range 0.15–0.18 over almost all conditions. For the dimensions of the SBWR suppression pool, the surface layer thickness will be approximately 0.3 m. If the velocity of

the surface layer is too high, so that inertia forces substantially exceed buoyancy forces, it will become unstable and expand to a thicker layer (Jirka and Harleman, 1979). Another Froude number characterizes the instability,

$$Fr_{surf} = \left[\frac{u_{surf}^2}{\beta_{pool} g (T_{surf} - T_{pool}) t_{surf}} \right]^{1/2} \quad (16)$$

The Froude number for the conditions in the SP indicate that the surface layer will be unstable in which case a hydraulic jump will occur and the surface layer will grow to a thickness of $t_{surf}/L_{sub} = 0.7$ or $t_{surf} = 1.5$ m. The distance over which this transition occurs is long compared with the pool width. Therefore, the surface layer will be in the transition phase as it moves across the pool.

In summary, when the vents clear, a portion of the liquid from the vents will be deposited along the surface of the SP in a 0.3–1.5 m thick layer. This effect is not important for the SBWR where the vent liquid is very close in temperature to the pool temperature. The liquid discharge phase is very brief; the liquid clears from the vents in approximately 1 s. However, the effects of the jet moving around the pool may be present for longer.

In some of the suppression pool simulation tests considered later, the liquid in the upper portions of the main vents was heated — in some cases to near saturation temperature — as a result of test preconditioning. For a worst case of saturated liquid in the vents, which occurs during preconditioning in experiments but not in actual reactors, the surface layer temperature could be 20 K above the average SP temperature. So, although this period is brief, it can provide an important part of the energy added to the surface of the pool if the liquid in the vents is initially warmer than the pool.

2.2. Noncondensible/steam injection

After the main vents clear, steam and noncondensible gases vent from the DW to the WW through the main vents. The timing and composition of the discharge are geometry and initial condition dependent. Integral system blowdown tests (Grafton and Seely, 1978) indicate an initial discharge with large noncondensible gas concentration that quickly decreases to a flow of predominantly steam as depicted in Fig. 2. In the case of the SBWR, there may be a longer period in which there is a combination of steam and noncondensible discharge from the vents as a result of less complete mixing in the more complicated DW geometry.

The noncondensible gases discharged into the pool are very buoyant. Although they are discharged at a high velocity, the buoyancy forces dominate and the noncondensible gases rise to the surface of the suppression pool causing significant pool swell (Varzaly et al., 1978). The buoyancy source and resulting plume can result in some circulation in the pool, however, in experiments, the noncondensible injection period is brief and results in very little circulation, mostly upward motion of the pool. In experiments, the noncondensibles introduce a negligible amount of energy to the pool since no condensation takes place. The steam injection period, which follows, lasts much longer and adds most of the energy deposited in the pool.

2.3. Steam discharge jet

Many researchers have looked at the condensation of steam discharged into pools and many complex models have been developed to predict pressure oscillations and the distance required for complete condensation of the steam (Weimer et al., 1973; Kudo et al., 1974; Cumo et al., 1978; Simpson and Chan, 1982; Tin et al., 1982; Nariai and Aya, 1986; Chun et al., 1996). For our purposes, the important result from this work is that the steam is condensed over a short distance (0.4–1.5 times the vent diameter) so that we can look at the liquid exiting the condensation region for its effects on the pool thermal behavior (Fig. 7). The important parameters for us then are the entrainment rate in this region and the momentum of the fluid exiting the region. A simplified analytical approach is described below.

The steam exiting the vent entrains liquid from the surrounding pool (Fig. 7). It is reasonable to assume that the high velocity steam will continue

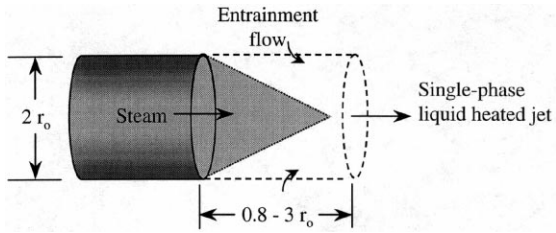

Fig. 7. Steam jet condensing at vent exit

moving horizontally resulting in a mixing region that maintain an approximately constant diameter as shown in the figure. Data from Kudo et al. (1974) show a diameter reduction of approximately 30% in the condensation region.

With the assumption of a constant mixing region diameter, conservation of momentum yields an equation for the average velocity of the jet exiting this condensing region

$$u_{\text{liq. jet}} = u_{\text{steam}}\sqrt{\frac{\rho_{\text{steam}}}{\rho_{\text{liq. jet}}}} \tag{17}$$

Typical steam and liquid velocities are 150 and 5 m s^{-1}, respectively. So there is a large reduction in the velocity. The entrainment ratio of pool flow to steam flow in this condensing process is approximately 30 = 1 so that the velocity and temperature of the steam discharge are reduced substantially.

An energy balance on the mixing region yields a relation for the enthalpy of the liquid exiting the mixing region

$$h_{\text{liq. jet}} = \frac{h_{\text{steam}}}{\phi} + \left(1 - \frac{1}{\phi}\right)h_{\text{pool}} \tag{18}$$

where ϕ is the ratio of flow exiting the mixing region to vent steam flow given by,

$$\phi = \frac{\dot{m}_{\text{liq. jet}}}{\dot{m}_{\text{steam}}} = \sqrt{\frac{\rho_{\text{liq. jet}}}{\rho_{\text{steam}}}} \tag{19}$$

For typical plant conditions the temperatures of steam, pool and liquid jet are,

$T_{\text{steam}} = 394$ K

$T_{\text{pool}} = 296$ K

$T_{\text{liq. jet}} = 317$ K

So the liquid is warmer than the pool by approximately 20 K.

Thus, for typical conditions, we have a liquid jet entering the pool with a diameter equal to the vent diameter, velocity on the order of 5 m s^{-1} and temperature about 20 K hotter than the pool. This condition is achieved within 1.5 diameters of the vent exit. The jet will move across the pool and hit the far wall taking mass and energy with it. This is the primary mechanism by which energy is transported around the pool.

The jet behavior is similar to that of the jet from vent clearing described above except that this jet more closely approaches a steady jet. The jet behavior can be predicted with the same relations used above.

As the steam flow through the vents diminishes, buoyancy eventually becomes dominant and the warm liquid rises as a buoyant plume. This occurs at very low steam flows so that the fraction of total energy input during the buoyant phase is quite low. The transition is given by Eq. (4) and occurs at a velocity of approximately 1.5 m s^{-1}. At low flow velocities and low noncondensible content, chugging can begin to occur.

Fig. 8 shows a flow regime map indicating the conditions for different types of flow to occur (Lahey and Moody, 1993). Chugging will commence at low flows and results in large oscillations in the steam-liquid interface (Fitzsimmons et al., 1979). Unlike condensation oscillations, chugging does cause large-scale motion in the pool and can enhance mixing. This work does not address the possible chugging phase of the transient.

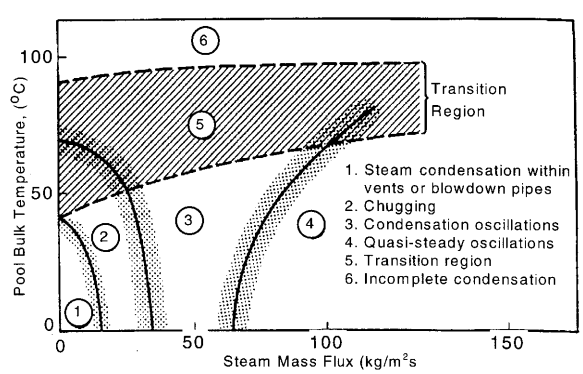

Fig. 8. Flow regime map for pure steam discharge.

3. Scaling

The descriptions above have identified some of the parameters that determine the behavior of jets in the SP. This section identifies some additional parameters that are important to SP behavior and thus should be considered when using scaled test facilities. Numerical values for the scaling parameters are shown in Table 1.

Scaling of test facilities to date (Varzaly et al., 1977, 1978, 1980) was done using the familiar power-to-volume full height scaling methodology as described by Yadigaroglu (1996). This results in one-to-one time scaling that ensures good top-down scaling of the facilities. As a result, mass and energy additions are proportional to mass and energy capacities of the system volumes. The energy scaling is characterized by the ratio of energy input to pool thermal capacity

$$\frac{\Delta E_{\mathrm{RPV}}}{E_{\mathrm{pool\ capacity}}} = \frac{\Delta(me)_{\mathrm{RPV}}}{m_{\mathrm{pool}} c_{\mathrm{p,pool}} \Delta T_{\mathrm{ref}}} \tag{20}$$

where $\Delta(me)_{\mathrm{RPV}}$ is the change in internal energy in the reactor pressure vessel (RPV) during blowdown, m_{pool} and $c_{\mathrm{p,pool}}$ are the mass and specific heat of the suppression pool and ΔT_{ref} is a reference value for the temperature change of the SP (taken as the subcooling). Since the DW acts as a passive surge volume between the RPV and WW, the vent mass and energy flow rates are approximately equal to those leaving the RPV, and the stored RPV energy discharged is used to represent the energy input to the pool.

The mass scaling is characterized by the ratio of mass injected into the SP to pool mass

$$\frac{\Delta m_{\mathrm{PRV}}}{m_{\mathrm{pool}}} \tag{21}$$

where again the RPV flow is taken as the flow into the SP. Since the RPV pressures are prototypical, we can neglect them in the scaling and represent the mass flow rate scaling as

$$\frac{\dot{m}_{\mathrm{RPV}}}{\dot{m}_{\mathrm{pool}}} \propto \frac{\rho_{\mathrm{o}} A_{\mathrm{choked}} u_{\mathrm{o}}}{m_{\mathrm{pool}}} \tag{22}$$

where A_{choked} is the critical flow area from the RPV to DW and ρ_{o} and u_{o} are reference density and velocities for the choked flow corresponding to the initial RPV pressure. Similarly, the rate of energy input into the pool is scaled by

$$\frac{\dot{E}_{\mathrm{RPV}}}{E_{\mathrm{pool\ capacity}}} = \frac{(\dot{m}h)_{\mathrm{RPV}}}{m_{\mathrm{pool}} c_{\mathrm{p,pool}} \Delta T_{\mathrm{ref}}} \tag{23}$$

In addition to the mean values in the pool, we are interested in the local temperatures that result from suppression pool stratification. To predict stratification in the pool, the behavior of local phenomena such as jet volumes and flow regime are important. These are characterized by the bottom-up scaling parameters. Many of these were defined in the previous section. Some additional bottom-up parameters are defined below.

The jet-to-pool volume-ratio characterizes how much of the fluid is in the jet versus in the ambient pool region. This can also be an indication of how much interaction the jet will have with other jets and the pool walls. For this purpose, the volume of the jet traversing the pool from the vent to the containment wall is used. It is given by,

$$\frac{V_{\mathrm{jet}}}{V_{\mathrm{pool}}} \tag{24}$$

which will characterize the fraction of the pool that is in the jets. This has an impact on both the residence time in the jet and how well defined the jets are.

The jet transit (or residence) time indicates the time it will take for energy and momentum to be transferred around the pool by the jets. The transit time is given by,

$$\tau_{\mathrm{jet}} = \frac{L}{\bar{V}} \tag{25}$$

where L is the length traveled and $\bar{V}$ is the average velocity in the jet. The transit time varies somewhat from one scale to another since the power to volume scaling results in one-to-one scaling of the velocities but the length scale varies with the square root of the facility scale. For reduced geometric scale tests, the transit time is much shorter than for full scale leading to accelerated time scaling for the distribution of energy.

For high Reynolds numbers and low buoyancy, the jet will mix the pool well. The pool Richardson number indicates when the inertia in a jet will

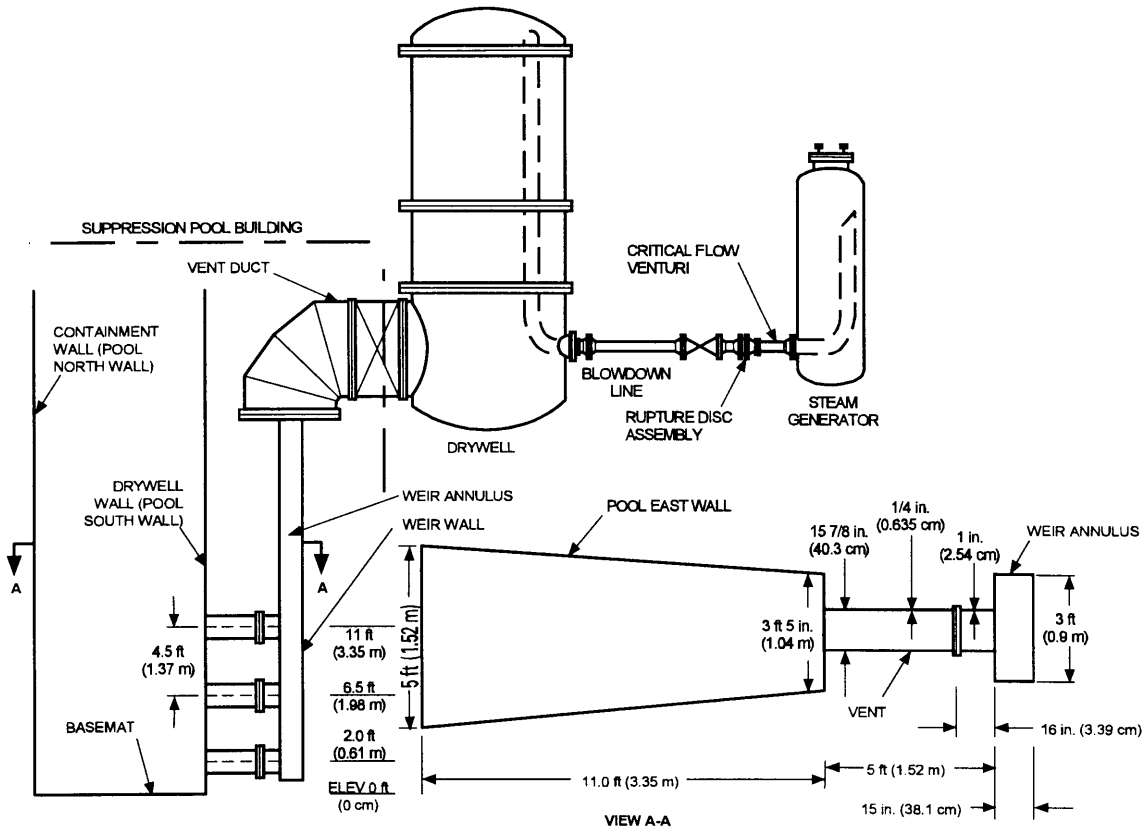

Fig. 9. PSTF test facility configure for test 5807-29.

cause stratification to break down in a pool (Jirka, 1982). This is given by,

$$Ri = \frac{Gr}{Re^2} = \left(\frac{\rho_a - \rho_{jet}}{\rho_a}\right)\frac{gD_o}{u_o^2}\left(\frac{H_{sf}}{D_o}\right)^2 \quad (26)$$

where H_{sf} is the depth of the stratified fluid in this case L_{sub}. For Ri less than 0.05, the inertial forces will overcome the buoyancy effects and the pool will become well mixed. However, the time constant to mix the pool can be very long. Therefore stratification may exist for a long time relative to the blowdown period as seen in the tests.

3.1. Scaled test facilities

As a part of a Mark III pressure suppression containment confirmatory test program, GE performed a series of full and reduced scale integral system tests in the pressure suppression test facility (PSTF). This test facility as configured for the different test series is described in more detail in Varzaly et al. (1977, 1978, 1980). The analysis described above was used to predict the surface temperatures in one of the tests from these test series in an effort to evaluate the effectiveness of the equations in predicting SP surface temperatures.

A schematic typical of the three test setups is shown in Fig. 9. In the PSTF test configuration, an electrically heated pressure vessel simulated the RPV. The RPV was connected to another pressure vessel — which simulated the DW, by a blowdown line — which included a critical flow venturi, rupture disc assembly, and a gate valve. The rupture disk in the blowdown pipe simulated the breaking of a main steamline, and the venturi upstream of the rupture disk set the size of the simulated break. The DW vessel was connected

via a discharge duct to a set of three Mark III horizontal vents, which discharged into a simulated sector of a Mark III suppression pool. The WW air space was open to the atmosphere, and this was done to simulate the large enclosed WW air space of the Mark III containment configuration.

The scaling parameters described above were evaluated for the SBWR and test facility to assess the applicability of these facilities in predicting the behavior of the SBWR SP. Table 1 presents the results. Despite the fact that they were designed for SP loading, the results indicate that the facility scaling is also good for thermal stratification modeling. The power-to-volume scaling used results in good scaling of both the top-down parameters relating mass and energy inputs to volume storage capacities and the bottom-up parameters defining the behavior of jets. The primary distortion comes from the reduced aspect ratio of the smaller scale experiments. This shows up in the volume and length of the jets relative to the SP volume. As a result the jet residence time is shorter in the small-scale facilities and the transit time for mass and energy moving around the pool through jets will be shorter. Consequently, the transition from a slightly stratified to a well-mixed pool progressed more quickly in the smaller experiments. Since the duration of these blowdown experiments was relatively short the full effect of this is not seen in the test data.

4. Application using TRACG

The concepts described in section 2 were implemented into a large system code, TRACG (Andersen et al., 1986) in an effort to predict the stratification in one of the scaled SP tests. The test is a one third scale test in the PSTF designated test, 5807-30 (Varzaly et al., 1977). The test consisted of an eight-degree segment of the suppression pool with three vents aligned vertically as shown in Fig. 9. The temperature data available for the test is too coarse to provide direct indication of the small-scale jet structures expected in the SP. However comparisons of the resulting pool temperatures can provide indirect evidence to confirm the behavior of jets within the pool.

TRACG does not have the ability to model small flow structures, such as jets and plumes, within its large volume cells. Therefore, auxiliary models are introduced to provide a mechanism to keep track of the mass and energy transport that occurs within the jet structures in the SP. When the momentum of entering fluid is weak the fluid will be deposited in the cell directly in front of the discharge pipe. For these periods the standard TRACG model is used. Past experience has shown that in these cases, TRACG can accurately predict the pool temperatures. Chugging only occurs at low mass fluxes so any chugging is modeled by the standard TRACG model, also.

In the PSTF test series the DW contained noncondensible gases in some tests and was purged with steam in others. When the DW has been purged with steam the discharge was clearly steam flow. For tests with noncondensibles in the DW the discharge was initially noncondensible gas and then shifted quickly to steam. Due to the clean cylindrical geometry of the DW vessel in the tests, the noncondensibles cleared rapidly from the DW. This is not true for a plant DW where the geometry is irregular. In actual plants more mixing of steam and noncondensible gases will occur in the DW and some of the noncondensibles will be held up in secluded areas of the DW resulting in a gradual release. Therefore, the transition from pure steam to pure vapor will be much slower in an actual plant containment.

4.1. Model implementation

When a strong discharge occurs, a TRACG 'control system', controlling distributed sources and sinks, is used to model the transport of mass and energy to different parts of the pool by jets. Fig. 10 shows the locations of the sources and sinks. The control system is set up to provide a simplified version of the jets described in the previous section. Basically, the entrained liquid from a cell is modeled as a 'sink'. The mass and energy deposited by the jet in a cell is modeled with a 'source'. The temperature and flow rate of the sources and sinks are set according to the jet models described in Section 2.3.

As the jet crosses ring 1, the cell closest to the discharge, it entrains fluid from ring 1. The jet then hits the far wall and spreads in the form of a radial jet. The radial jet collides with jets from surrounding vents in the horizontal direction (or walls in the case of the segment tests) and in the vertical direction when the vent above or below is also open. As a result of this interaction, it is assumed that half of the radial jet is deposited in the cell opposite the vent discharge, ring 2 of that elevation. The discharged fluid will contain half of the fluid discharged from the vent plus half of the fluid entrained as the jet passed through ring 1. The entrainment is calculated according to Eqs. (10) and (19).

For the top vents (level 3), 25% of the jet is deposited in the cell immediately above the discharge elevation (level 4, ring 2). This represents the remaining fluid broken up by collision with surrounding jets. Again, this flow contains vent discharge flow and entrained flow from ring 1. The additional entrainment in ring 2 is neglected because it is negligible compared with the entrainment from ring 1. Recall that the entrainment ratio of the exiting steam jet is approximately 30:1, while the additional entrainment from traversing the entire pool is only about 2.3:1.

The last 25% of the jet flow travels up along the containment wall in the form of a wall jet and is deposited in the top layer of the pool (level 5, ring 2). The top layer thickness is set to match the expected thickness of the surface layer that moves across the pool (Section 2.1.2).

For the lower two vents, the second half of the jet flow is deposited in the ring above the discharge elevation in ring 2 as shown in Fig. 10. This represents the remainder of the flow that was halted due to interactions with adjacent jets and structures. For these lower vents, the vent above will always be open so there will be no open path to flow up along the wall towards the surface as the top vent flow does.

When the discharge jets become weak, the jet model is shut off and the model reverts back to the standard TRACG model. The standard TRACG model deposits all fluid into the cell closest to the discharge. It does not model the effects of jets in the suppression pool. The transition is determined using Eq. (4). When the transition distance to a buoyant jet, as calculated by Eq. (4), is less than the width of ring 1, the jet model is turned off.

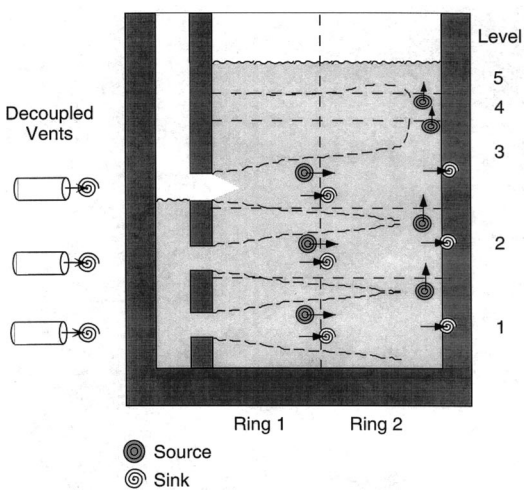

Fig. 10. TraCG sources and sinks used to model jets in suppression pool.

4.2. Calculations and results

Test 5807-30 is a one-third-scale test of a large sized steam break. Data is available for the first 40 s of the transient. The top horizontal vent remains open throughout this period. The middle and bottom vents close at 16 and 4 s, respectively. The results obtained with the modified TRACG model are compared against the test data in Figs. 11–14.

Fig. 11 shows the temperature profiles in the inner and outer ring of the pool, respectively, at various times. Values are shown both from test data and TRACG predictions. The test data plots are obtained by averaging together thermocouple readings in each region of the pool. The number of thermocouples in each region varies from one to seven. The smooth profile comes from using a smoothing function — there are no points in between those shown in the curves.

The profiles show that the jet quickly penetrates across the pool and transfers energy to the upper layers of the pool as described in Section 2. The TRACG model implementation shows the same

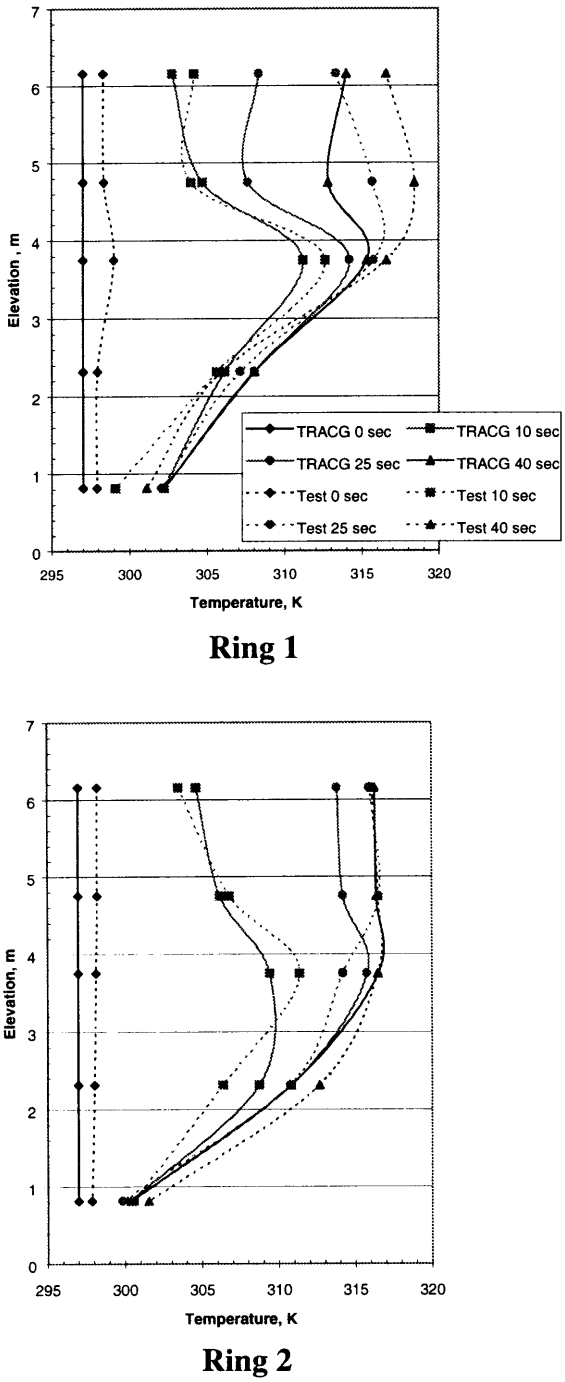

Fig. 11. Temperature profiles development in suppression pool.

trends but has a time lag in depositing the energy in the top two layers, especially in ring 1. This is probably because a jet model to carry the energy back along the surface layer was not implemented. Instead, the jet energy was deposited in ring 2 as described previously.

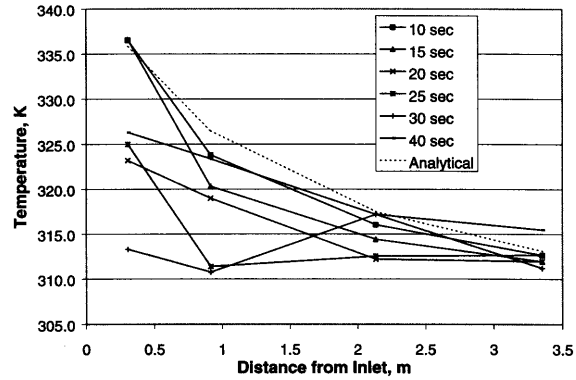

Fig. 12. Temperature decay of top vent jet as it moves across pool.

Fig. 12 shows the decrease in jet temperature as it moves across the pool from the top vent. An analytical prediction using the equations in Section 2 is shown also. As indicated by the good agreement, the simple correlations for jet entrainment give a good approximation. It is likely that the predictions will be less accurate as the jet spreads along the wall and pool surface because of uncertainties in the interactions with walls. There are no data available within the thin jet boundary layers along the wall and pool surface for comparison.

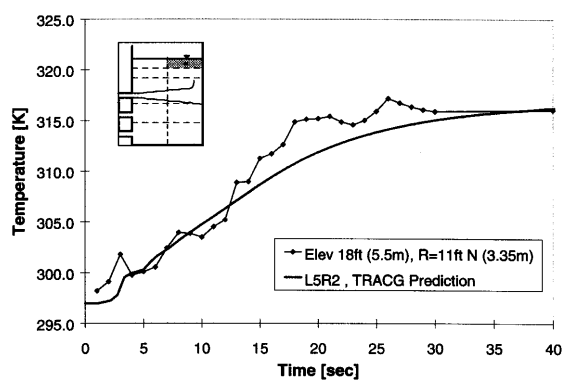

Fig. 13. Test 5807-30, SP temperatures in Level 5, Ring 2 (pool surface).

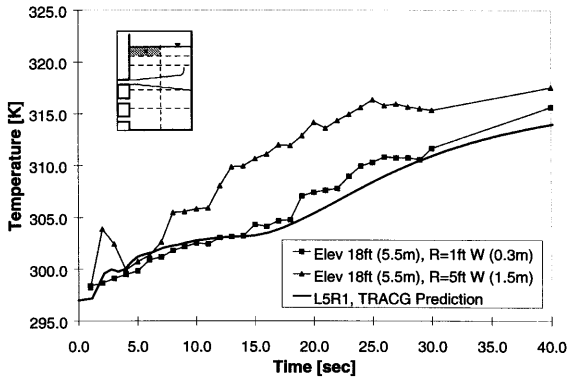

Fig. 14. Test 5807-30, SP temperatures in Level 5, Ring 1 (pool surface).

It appears from the test data in Fig. 11 that the pool is well mixed in the region above the top vent. However, this is partially an artifact of averaging the thermocouple measurements in each region. Figs. 13 and 14 show individual thermocouple readings for the top elevation of the pool. As shown in the ring 1 data, there is a significant variation even within one region. The resolution in the TRACG model does not allow these variations to be captured. In the plots, the appropriate thermocouple data is plotted along with the TRACG predictions. A diagram of the suppression pool in each figure indicates the location of the plotted temperatures. Small square and triangle shapes indicate the approximate location of the thermocouples used in the test, and the gray region indicates the node plotted for TRACG.

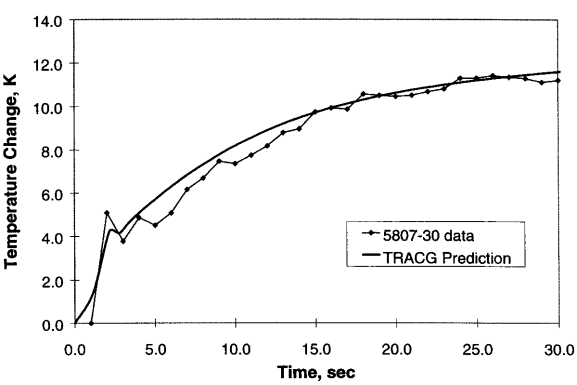

Fig. 15. Test 5807-30, suppression pool mixed mean temperature increase.

Fig. 15 shows the increase in mixed mean temperature in the entire pool. The values for the test are estimated using the available data. Energy in the pool should be a monotonically increasing function. The oscillations are an indication of the range of uncertainty in the estimation. The error results because each thermocouple temperature is used to represent the temperature for a large portion of the pool where there might be significant temperature variations. The energy input from the TRACG simulation compares well with the energy input estimated from the data.

Test 5807-30 was initiated by purging the DW vessel with steam for an extended period of a few hours. As a result, the fluid in the upper portion of the weir was heated to near saturation temperature. This is indicated by the early temperature peak in the upper levels of the pool that is shown in much of the thermocouple data. The temperatures in the weir region were not available so they had to be estimated using the energy balance for the pool. The TRACG weir temperatures were initialized to match the pool energy early in the transient. Once this was done, the energy balance for the remainder of the transient matches the data well.

5. Conclusions

Energy transport in the suppression pool of pressure suppression containments during the blowdown period of a loss-of-coolant accident is a high-energy, 3-D event. However, substantial qualitative understanding of the energy transport mechanisms in the suppression pool is gained by the use of analytical models. Integral formulations of well-known free-jet structures are used to construct a model to predict the influence of steam and liquid jets issuing from the main vents on thermal stratification in the pool. In doing so, interactions between adjacent jets have been neglected. The insight gained from the simplified models provides both an understanding of the scaling for pool mixing tests as well as the key parameters controlling the evolution of the pool surface temperatures.

To assess the usefulness of this simplified treatment, the analytical models are implemented into a system simulation code, TRACG, and used to model thermal stratification behavior in a scaled test facility. The results show good general agreement with the test data, however, the sparseness of the experimental data does not allow verification of the detailed local behavior in the pool.

The analysis and data show that steam jets provide the majority of energy added to the pool. Past reviews of the test data have shown that the horizontal steam jets do not mix appreciably with the pool below the level of the jets so that calculating the pool bulk temperature based on the pool volume above the jets results in a rough estimate of the pool temperature. This work further shows that steam jets are expected to entrain pool liquid at a rate greater than 50 times the jet steam injection mass flow rate before reaching the pool surface. Thus, the surface layer of the pool will not be substantially hotter than the bulk pool temperature calculated for the pool region above the jet injection point. Therefore, there is little concern about forming a hot surface layer. Future efforts in this area could be directed at improving the estimates of entrainment in the condensing jet region since this parameter is dominant in affecting the pool surface temperature.

Acknowledgements

This work was carried out with partial funding from the Electric Power Research Institute under the Advanced Light Water Reactor program.

Appendix A. Nomenclature

A	area
a	distance from jet virtual origin to end of pipe (see Fig. 4)
c_p	specific heat
d	thickness of radial wall jet
D	diameter
E	energy
$\dot{E}$	energy rate
e	specific energy
Fr	Froude number
g	gravity force
Gr	grashof number
H	distance from vent to opposite wall, height
h	specific enthalpy
L	length
m	mass
$\dot{m}$	mass flow rate
Q	volumetric flow rate
Re	Reynolds number
Ri	Richardson number
r	radial distance
T	absolute temperature
t	thickness of layer
u	velocity
V	volume
$\bar{V}$	average velocity
x	axial distance along jet
Z	distance along radial wall jet
α_t	Taylor's entrainment constant
β	thermal coefficient of expansion
δ	wall jet thickness
η	similarity variable
v	kinematic viscosity
ϕ	mass flow ratio
ρ	mass density
τ	time constant

Subscripts

1/2	position where axial velocity equals 1/2 of centerline velocity
a	ambient
c	condensation
e	entrainment
imp	impingement
o	jet exit
r	radial distance
sub	submergence
surf	surface
trans	point of transition from forced to buoyant

Acronyms

CFD	computational fluid dynamics
DW	drywell
ESBWR	european simplified boiling water reactor

LOCA	loss-of-coolant accident
PCC	passive containment cooling
PSTF	pressure suppression test facility
RPV	reactor pressure vessel
SBWR	simplified boiling water reactor
SP	suppression pool
SRV	safety relief valve
WW	wetwell

References

Andersen, J.G.M., Shaug, J.C., Shiralkar, B.S., 1986. TRAC Developments at General Electric. Proceedings of the 14th Water Reactor Safety Meeting, vol. 5 NUREG/CR-0082.

Chun, M., Kim, Y., Park, J., 1996. An investigation of direct condensation of steam jet in subcooled water. Int. Comm. Heat Mass Transfer 23, 947–958.

Coddington, P., Andreani, M., 1995. SBWR PCC vent phenomena and suppression pool mixing. Seventh International Topical Meeting on Nuclear Reactor Thermal Hydraulics.

Cumo, W., Farello, G.E., Ferrari, G., 1978. Direct heat transfer in pressure–suppression systems. Proc. Sixth Int. Heat Transfer Conf. 5, 101–106.

Dodge, F.T., Ricker, R., 1978. Flow of liquid jets through closely woven screens. AIAA J. Spacecraft/Rockets 15, 213–218.

Fitzsimmons, G.W., Galyard, D.L, Nixon, R.B., Mann, M.J. & Yu, K.P., Mark I Containment Program, Full Scale Test Program Final Report, General Electric Report, NEDE-24539, August 1979.

Gauntner, J.W., Livingood, J.N.B., Hrycak, P., Survey of literature on flow characteristics of a single turbulent jet impinging on a flat plate. NASA TND-5652, February 1970.

Gebhart, B., Jaluria, Y., Mahajan, R.L., Sammakia, B., 1988. Buoyancy Induced Flows and Transport. Hemisphere, New York.

Grafton, W.A., Seely, D.S., Mark III Condensation oscillation data analysis and correlations. General Electric Report, NEDE-23972, October 1978.

Hinze, J.O., 1959. Turbulence: An Introduction to Its Mechanism and Theory. McGraw-Hill, New York.

Jirka, G.H., 1982. Turbulent buoyant jets in shallow fluid layers. In: Rodi, W. (Ed.), Turbulent Buoyant Jets and Plumes. Pergomon Press, New York.

Jirka, G.H., Harleman, D.R.F., 1979. Stability and mixing of vertical plane buoyant jet in confined depth. J. Fluid Mech. 94, 275–304.

Kudo, A., Egusa, T., Toda, S., 1974. Basic study on vapor suppression. Proc. Fifth Int. Heat Transfer Conf. 3, 221–225.

Lahey, R.T., Moody, F.J., 1993. The Thermal Hydrualics of a Boiling Water Reactor, second ed. American Nuclear Society, Illinois], p. 582.

Nariai, H., Aya, I., 1986. Fluid and pressure oscilations occurring at direct contact condensation of steam flow with cold water. Nucl. Eng. Des. 95, 35–45.

Peterson, P.F., 1994. Scaling and analysis of mixing in large stratified volumes. Int. J. Heat Mass Transfer 37 (Suppl. 1), 97–106.

Poreh, M., Tsuei, Y.G., Cermak, J.E., 1967. Investigation of a turbulent radial wall jet. J. Appl. Mech. 2 (34), 457–463.

Rajaratnam, N., 1976. Turbulent Jets. Elsevier, New York, p. 14.

Schlichting, H., 1960. Boundary Layer Theory. McGraw-Hill, New York, p. 608.

Sfier, A.A., 1976. The velocity and temperature fields of rectangular jets. Int. J. Heat Mass Transfer 19, 1289–1297.

Simpson, M.E., Chan, C.K., 1982. Hydrodynamics of a subsonic vapor jet in subcooled liquid. J. Heat Transfer 104, 271278.

Tin, G.D., Lavagno, E., Malandrone, M., 1982. Pressure and temperature measurements in a vapour condensing jet. Proc. Seventh Int. heat Transfer Conf. 6, 159–164.

Upton, H.A., Torbeck, J.E., Billig, P.F., Duncan, J.D., Herzog, M., 1996. SBWR design update: passively safe, nuclear power generation for the twenty first century. Fourth International Conference on Nuclear Engineering (ICONE-4) vol. 2, pp. 379–394.

Varzaly, A.M., Grafton, W.A., Chang, H., Mitchell, M.K., Mark III, 1977. Confirmatory test program, $1/\sqrt{3}$ scale condensation and stratification phenomena-test series 5807. General Electric Report, NEDE-21596-P, March 1977.

Varzaly, A.M., Grafton, W.A., Seely, D.S., Mark III, 1978. Confirmatory test program, full scale condensation and stratification phenomena-test series 5707. General Electric Report, NEDE-21853-P, August 1978.

Varzaly, A.M., Yu, K.P., Kerinenen, J.A., Mark III, 1980. Confirmatory test program, 1/9 area scale multicell condensation and stratification phenomena-test series 6003. General Electric Report, NEDE-24720-P, January 1980.

Weimer, J.C., Faeth, G.M., Olson, D.R., 1973. Penetration of vapor jets submerged in subcooled liquids. Am. Inst. Chem. Eng. J. 19 (3), 552–558.

Yadigaroglu, G., 1996. Derivation of general scaling criteria for BWR containment tests. Fourth International Conferance on Nuclear Engineering (ICONE-4) vol. 1, Part B., pp. 843–851.